Bull. Mater. Sci. (2021)44:198
https://doi.org/10.1007/s12034-021-02472-9

Enhancing the absorption of 1-chloro-1,2,2,2-tetrafluoroethane on carbon nanotubes: an *ab initio* study

MOHSEN DOUST MOHAMMADI[1], HEWA Y ABDULLAH[2,*], GEORGE BISKOS[3,4] and SOMNATH BHOWMICK[3]

[1] School of Chemistry, College of Science, University of Tehran, 14176 Tehran, Iran
[2] Physics Education Department, Faculty of Education, Tishk International University, 44001 Erbil, Iraq
[3] Climate and Atmosphere Research Centre, The Cyprus Institute, 2121 Nicosia, Cyprus
[4] Faculty of Civil Engineering and Geosciences, Delft University of Technology, 2628 CN Delft, The Netherlands
*Author for correspondence (hewayaseen@gmail.com)

MS received 7 December 2020; accepted 24 February 2021

Abstract. We have investigated the possibility of utilizing various single-walled pristine and doped carbon nanotubes as adsorbents for the 1-chloro-1,2,2,2-tetrafluoroethane (HCFC-124) gaseous molecule. Three candidates, including pristine carbon nanotube (CNT), silicon carbide nanotube (SiCNT) and germanium-doped SiCNT (SiCGeNT) are identified and evaluated theoretically. The quantum simulations have been performed at the density functional theory (DFT) level with four different functionals (i.e., M06-2X, ωB97XD, CAM-B3LYP and B3LYP-D3) with a split-valence triple-zeta basis set (6-311G(d)). We found that adsorption on the SiCGeNT is most favourable, while that on the pristine CNT yields the lowest adsorption energy. Adsorption on these nanotubes is not accompanied by an active charge-transfer phenomenon; instead, it is driven by weak van der Waals forces. The HOMO–LUMO energy gaps drastically change when the dopant atom is added to the SiCNT, thereby improving their overall adsorption capability. Among all of the adsorbents investigated here, SiCGeNT shows the most favourable for designing effective HCFC-124 nanosensors.

Keywords. Silicon carbide nanotube; 1-chloro-1,2,2,2-tetrafluoroethane; HCFC-124; freon 124; natural bond orbital.

1. Introduction

HCFC-124 (1-chloro-1,2,2,2-tetrafluoroethane; C_2HClF_4) is a partially halogenated chlorofluorocarbons (CFCs) that is currently employed as an alternative to CFCs with a high ozone depletion potential [1]. Also known as the Suva 124 refrigerant or FE-241 fire extinguishant in the industry, it is commonly used in air conditioning systems, refrigerators and gaseous fire suppression systems. Nevertheless, HCFC-124 is still listed among the gases that contribute towards the depletion of stratospheric ozone [2], while at the same time, it is considered as a greenhouse gas with high global warming potential [3], warranting for a phase out of its emissive uses in developed and developing countries [4–6]. This, in turn, motivates the development and exploitation of selective sensors that can efficiently detect potential emissions of HCFC-124 in the atmospheric environment. For instance, a wide range of nanomaterials have been developed and tested for gas sensors that can have low limits of detection, high measurement accuracy, low response time, resistant to variable environmental conditions, as well as low production cost [7–17].

Among the different types of sensors, those that rely on the adsorption of the target gas molecules on specific sites of sensing materials, with a subsequent change in their properties, provide a rather promising solution as they can be designed in compact and cost-effective manners. Numerous efforts have been made to understand and improve the adsorption process in sensing nanomaterials. Approaches including metal doping [18–20], surface defects [21–23] and transition metal decoration [24,25], have been investigated among others. Nanotubes have been extensively studied as potential adsorbents in sensing nanomaterials. Lin *et al* [26] made a comprehensive study on the effect of transition metal decoration on boron nitride nanotubes, whereas elements, such as aluminium, gallium and germanium have been widely used as a spread on nanotubes overall [27–30]. Other studies have shown that even the introduction of non-metal atoms, such as oxygen, can activate the overall surface of nanomaterials [31]. In general, impurity-decorated nanomaterials, with a reduced electrical resistance compared to their pure counterparts, can enhance the sensitivity and overall performance of gas sensors [32].

Here, we report a comprehensive study on the intermolecular interactions of HCFC-124 gas molecule with pristine carbon nanotube (CNT), silicon carbide nanotube (SiCNT) and Ge-doped silicon carbide nanotube (SiCGeNT)

Published online: 01 July 2021

using *ab initio* calculations at the density functional theory (DFT) level. The rest of the paper is organized as follows. Section 2 provides all the computational details, whereas section 3 discusses the results of our study in four subsections: 3.1, providing insights about the bond length and other geometrical properties; 3.2, where we discuss the density of states (DOS) and other molecular properties as well as 3.3 and 3.4, that discusses the nature of intermolecular interactions between two fragments (gas and nanotubes). The conclusions of this study are summarized in section 4.

2. Computational details

Optimized geometries of the nanotube structures have been obtained through the Kohn–Sham DFT [33–36] with two-dimensional periodic boundary conditions (PBC–DFT). In total, we have used four functionals, including M06-2X [37], ωB97XD [38], the B3LYP-D3 scheme of Grimme [39–41], and the Coulomb attenuating method (CAM)-B3LYP [42,43]. A split-valence triple-zeta basis sets with d-type Cartesian–Gaussian polarization functions (6-311G(d)) have been employed. As reported by Goerigk and Grimme [44], choice of the basis set is appropriate for the systems under consideration. For all calculations, sampling in the Brillouin zone [45] has been performed with a $3 \times 1 \times 1$ k points. The kinetic energy cutoff has been set to 450 eV. The full-dimensional geometry optimization calculations have been performed with Berny's [46] optimization procedure as included in the Gaussian 16 Rev.C.01 [47] package with default convergence criteria. Additional frequency calculations have been carried out on the local minima to determine the nature of the stationary points. Natural bond orbital (NBO) calculations have performed to determine the probable existence of the charge-transfer phenomenon between occupied and unoccupied orbitals. The Multiwfn [48] package has been employed for the NBO, non-covalent interaction (NCI) and quantum theory of atoms in molecule (QTAIM) analyses. DOS diagrams have been created with the GaussSum [49] program.

The energy of adsorption (E_{ads}) between the two fragments (nanotube and HCFC-124) can be calculated as:

$$E_{ads} = E_{tube/HCFC\text{-}124} - E_{tube} - E_{HCFC\text{-}124} + \Delta E_{(BSSE)}, \quad (1)$$

where $E_{tube/HCFC\text{-}124}$ is the total energy of the gas/nanotube cluster at its optimized geometry, E_{tube} and $E_{HCFC\text{-}124}$ are the energies of the isolated nanotube and isolated HCFC-124 molecule, respectively. $\Delta E_{(BSSE)}$ is the basis set superposition error (BSSE) correction obtained through the Boys and Bernardi's counterpoise procedure [50,51]. According to equation (1), negative values of E_{ads} (i.e., exothermic adsorptions) correspond to a stable complex, whereas positive values indicate that the adsorption is not favoured.

3. Result and discussion

3.1 *Geometric surveys*

The ωB97XD functional has been selected as the preferred method for the initialization of the geometry optimization process for both the isolated systems as well as the complex structures. They are later re-optimized using the other three functionals; viz. M06-2X, CAM-B3LYP and B3LYP-D3. All these functionals offer many advantages and corrections. For example, the B3LYP-D3 functional, also known as D3 (BD) (GD3BJ), developed by Grimme *et al* [39–41], includes dispersion correction. The global hybrid functional with double non-local exchange (i.e., M06-2X [37]) is a high-performance method to study the non-covalent interactions. On the other hand, the ωB97XD functional does account for the effect of long-range interactions as well as the dispersion corrections [38].

The PBC–DFT framework at the ωB97XD/6-311G(d) level has been applied on a pristine unit cell of $C_{30}C_{30}$ (CNT) with a length and diameter of 7.36 and 6.80 Å, respectively, and $Si_{30}C_{30}$ (SiCNT) with a length and of 9.28 Å and a diameter of 8.50 Å. Figure 1 illustrates the unit cell of pristine CNT and SiCNT. These unit cells are expanded three times along with its central axis, and the optimization calculations are repeated at the same level of theory. It should be noted that the boundary effects have been reduced by terminating the terminal atoms with H atoms. For the case of SiCGeNT, one of the Si atoms has been substituted by a Ge atom on the optimized geometry of SiCNT. The optimized values of the various bond lengths of CNT, SiCNT and SiCGeNT are shown in figure 2. Evidently, the C–C bond length in CNT falls within 1.43–1.41 Å (cf. figure 2a). Similarly, the Si–C and Ge–C bond lengths in SiCNT and SiCGeNT are 1.78 and 1.84 Å, respectively (cf. figure 2b and c). Due to the inner stress, the Si–C bond lengths within the vicinity of the Ge dopant atom vary between 1.77 and 1.79 Å (figure 3).

For the simulations of HCFC-124 adsorption on the surface of CNT, SiCNT and Ge-doped SiCNT, the gas

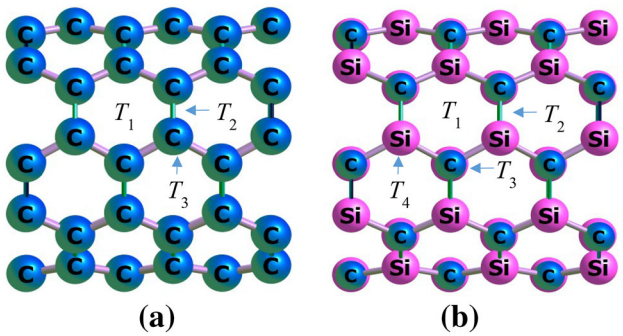

Figure 1. Unit cells of (**a**) carbon nanotube (CNT) and (**b**) silicon carbide nanotube (SiCNT).

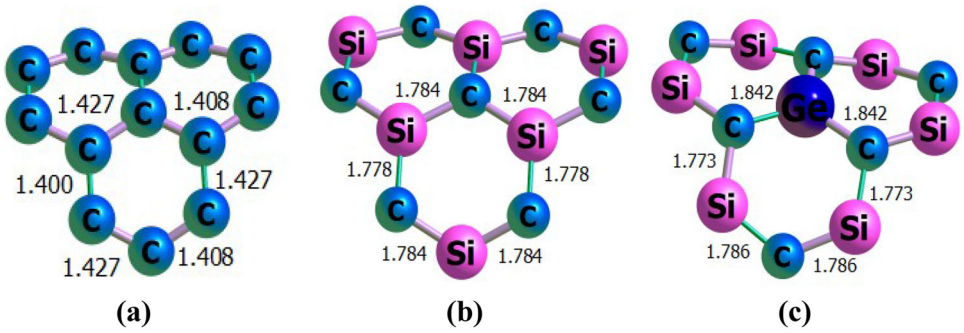

Figure 2. Bond lengths (expressed in Å) of (**a**) pristine carbon nanotube (CNT), (**b**) silicon carbide nanotube (SiCNT) and (**c**) Ge-doped silicon carbide nanotube (SiCGeNT) obtained at ωB97XD/6-311G(d) level of theory.

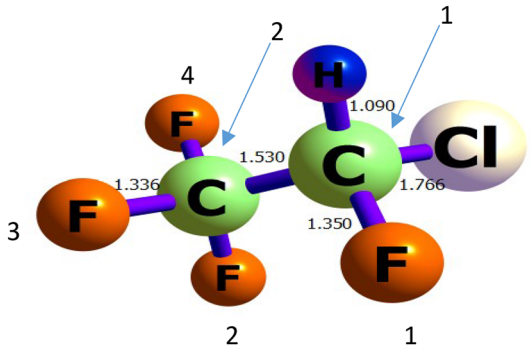

Figure 3. Optimized geometry of the 1-chloro-1,2,2,2-tetrafluoroethane (HCFC-124) molecule obtained at the ωB97XD/6-311G(d) level of theory.

molecule has been placed on top of the nanotube at various positions and several different orientations to find the local minima. HCFC-124 has three different types of atoms (viz. H, Cl and F) through which it can bind with the nanotubes. For CNTs and SiCNTs, there are respectively, three and four different sites of adsorption as illustrated in figure 1. Those include sites T_1 in the middle of the hexagonal ring, T_2 between Si and C atoms (between two C atoms), T_3 on top of C atom and T_4 on top of Si atom. The gas molecule has been put on top of each T_x site at various distances and the optimization calculations have been initiated at the PM7/6-311G(d) level. It should be stressed that overall, there are $6 \times 4 \times 10 = 240$ different initial orientations. For SiCNT, the six different heads of the gas molecule are put on each of the four sites of the nanotube ranging from the vertical distances of 0.5–5.0 Å (with 0.5 Å intervals). Similarly, the heads are put on top of three different sites, resulting in 180 initial geometries for the CNT. From these calculations, 12 and 3 minima are respectively, identified for SiCNT and CNT. The optimized structures of all complexes obtained at the ωB97XD/6-311G(d) level are depicted in figure 4. The most stable complexes of the ωB97XD computations are then re-optimized with other functionals.

The adsorption energies calculated by the four functionals are listed in table 1. The adsorption energies obtained from the ωB97XD and B3LYP-D3 methods are in good agreement with each other. The adsorption energy calculated by the B3LYP-D3 functional is the largest among all other functionals. The largest adsorption energy has been obtained on the surface of SiCGeNT (−0.775 eV). This indicates that the reactivity of HCFC-124 is maximum on the Ge-doped nanotube. On the other hand, the reactivity of HCFC-124 with pristine CNT has the weakest interaction (low adsorption energy) among all nanotubes. To reduce computational cost, further analyses have been performed with the results obtained at the ωB97XD/6-311G(d) level of theory.

3.2 *Electronic structure*

The 'conceptual DFT' has been developed to consider the reactivity concept. Various electronic properties can be obtained from the HOMO–LUMO energy gap (HLG) [52] using DFT calculations. When an external potential applied to a system, the energy within the Hohenberg–Kohn theorem [33] context, changes as follows:

$$\begin{aligned}\Delta E &\equiv E[N+\Delta N, v(\mathbf{r})+\Delta v(\mathbf{r})] - E[N, v(\mathbf{r})] \\ &= \left(\frac{\partial E}{\partial N}\right)_v \Delta N + \int \left(\frac{\delta E}{\delta v(\mathbf{r})}\right)_N \delta v(\mathbf{r}) d(\mathbf{r}) \\ &\quad + \frac{1}{2!}\left\{\left(\frac{\partial^2 E}{\partial N^2}\right)_v \Delta N^2 + 2\int \left(\frac{\partial}{\partial N}\left(\frac{\delta E}{\partial v(\mathbf{r})}\right)_N\right)_v \Delta N \delta v(\mathbf{r}) \right. \\ &\quad \left. + \iint \left(\frac{\partial^2 E}{\partial v^2(\mathbf{r})}\right)_N \delta v(\mathbf{r}) \delta v(\mathbf{r}') d\mathbf{r} d\mathbf{r}'\right\} + \cdots \end{aligned} \quad (2)$$

In the above Taylor expansion, N is a global quantity and $v(\mathbf{r})$ a local function. The HOMO and LUMO energies are related to the ionization energy and electron affinity. Other properties, such as the electronegativity (χ), chemical

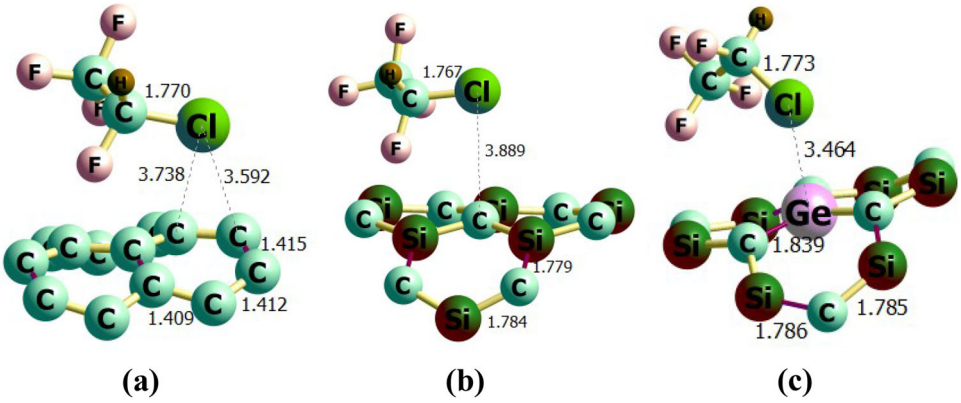

Figure 4. Optimized structures of (**a**) HCFC-124/CNT, (**b**) HCFC-124/SiCNT and (**c**) HCFC-124/SiCGeNT complexes obtained at the ωB97XD/6-311G(d) level of theory.

Table 1. Basis set superposition error (BSSE) corrected adsorption energies (E_{ads}) of the HCFC-124/nanotube complexes. All E_{ads} values are reported in eV and obtained from the geometry optimization calculations using CAM-B3LYP, M06-2X, ωB97XD and B3LYP-D3 functionals in combination with a 6-311G(d) basis set.

Systems	ωB97XD	CAM-B3LYP	M06-2X	B3LYP-D3
C_2HClF_4/CNT	−0.100	−0.015	−0.032	−0.110
C_2HClF_4/SiCNT	−0.431	−0.273	−0.385	−0.537
C_2HClF_4/SiCGeNT	−0.675	−0.498	−0.640	−0.775

potential (μ) and the electrophilicity index (ω) are also related to the HOMO–LUMO energies as follows:

$$-\chi = \left(\frac{\partial E}{\partial N}\right)_v = \mu \cong \frac{(\varepsilon_{\text{LUMO}} + \varepsilon_{\text{HOMO}})}{2}, \tag{3}$$

$$\eta = \left(\frac{\partial \mu}{\partial N}\right) = \frac{1}{2}\left(\frac{\partial^2 E}{\partial N^2}\right)_v = \frac{1}{2}(IP - EA), \tag{4}$$

$$\omega = \frac{\mu^2}{2\eta}. \tag{5}$$

The values of these properties as calculated at the ωB97XD/6-311G(d) level are listed in table 2. Evidently, the HLG decreases after adsorption. The decrease in HLG is more pronounced on CNT than other doped nanotubes. For example, the decrease in the HLG on CNT is about 0.26 eV, whereas for the SiCNT and SiCGeNT, the respective values are around 0.07–0.08 eV. The decrease in HLG may be attributed to two distinct phenomena. The HOMO energy is decreased, while at the same time, the LUMO is stabilized. This simultaneous increase and decrease in the HOMO–LUMO are about the same amount, except for SiCGeNT. The stabilization energy of LUMO in SiCGeNT is more than two times the amount of destabilization energy of the HOMO. In principle, we can attribute the changes in the HLG's due to a small charge-transfer from the HOMO to LUMO during adsorption. The DOS map is useful in intuitively revealing the density of distribution of molecular orbitals in different energy regions. The changes in the HOMO–LUMO energy gaps on adsorption can be directly inferred from such a map (cf. figure 5). Since there is a decrease in the HLG values due to adsorption, the resistivity of the material will decrease (as it is proportional to the reciprocal of the conducting electron population). As a result, the electric current generated on the adsorbed complex will face the lowest resistance. The effect on the chemical potential μ due to adsorption is more complex. It decreases slightly for CNT, while it remains the same for SiCNT and increases for the SiCGeNT nanotube. Finally,

Table 2. HOMO energy (ε_H), LUMO energy (ε_L), Fermi energy (E_F), HOMO–LUMO energy gap (HLG), chemical potential (μ), chemical hardness (η) and electrophilicity (ω). All values are given in eV and have been obtained at the ωB97XD/6-311G(d) level of theory.

Systems	ε_H	ε_L	E_F	HLG	μ	η	ω
CNT	−4.370	−3.430	−3.900	0.941	−3.900	0.470	3.577
SiCNT	−5.356	−1.917	−3.636	3.439	−3.636	1.719	11.368
SiCGeNT	−5.352	−1.937	−3.644	3.415	−3.644	1.707	11.338
C_2HClF_4/CNT	−4.240	−3.556	−3.898	0.684	−3.898	0.342	2.598
C_2HClF_4/SiCNT	−5.320	−1.952	−3.636	3.368	−3.636	1.684	11.131
C_2HClF_4/SiCGeNT	−5.325	−1.993	−3.659	3.332	−3.659	1.666	11.154

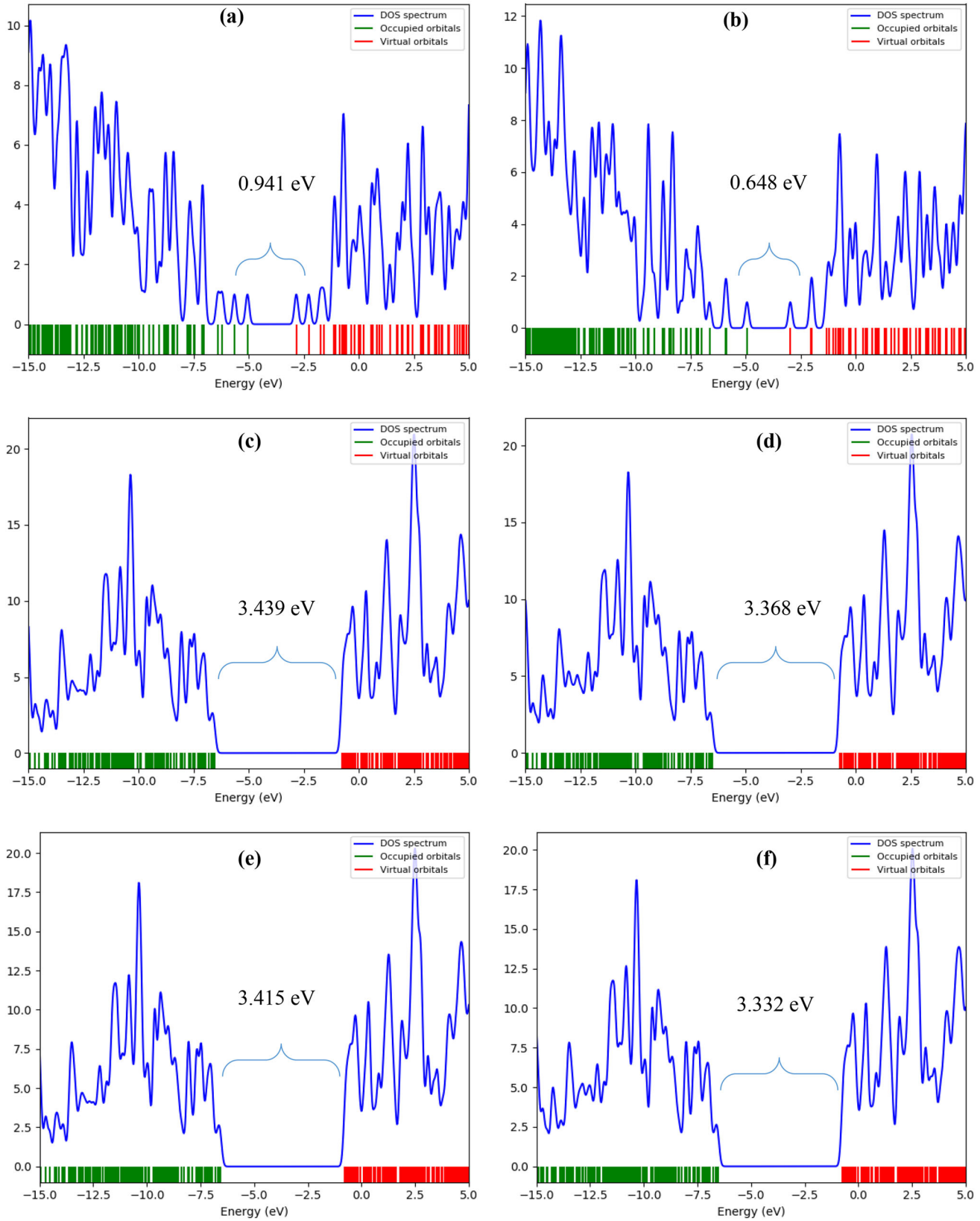

Figure 5. Density of state maps for (**a**) CNT, (**b**) HCFC-124/CNT, (**c**) SiCNT, (**d**) HCFC-124/SiCNT, (**e**) SiCGeNT and (**f**) HCFC-124/SiCGeNT. Diagrams are obtained using the ωB97XD/6-311G(d) level of theory.

the values of both chemical hardness (η) and the electrophilicity index (ω) decrease upon adsorption.

Table 3. Values of Mulliken, Mayer and Wiberg bond orders obtained from the interactions between the HCFC-124 molecule, and CNT, SiCNT and SiCGeNT. All calculations have been carried out at the ωB97XD/6-311G(d) level of theory.

Systems	X[a].....Y[b]	Mulliken	Mayer	Wiberg
C_2HClF_4/CNT	Cl–C	0.102	0.143	0.115
C_2HClF_4/SiCNT	Cl–C	0.117	0.234	0.247
C_2HClF_4/SiCGeNT	Cl–Ge	0.171	0.271	0.236

[a]X atom belongs to HCFC-124.
[b]Y atom belongs to the nanotube.

3.3 *NBO analysis*

The NBO method, developed by Weinhold *et al* [53–55], is one of the most accurate population analysis methods. According to this, the distribution of electron density between atoms in bonds are evaluated. The term NBO refers to a bonding orbital with the maximum electron density. A density matrix, calculated by DFT, and the atomic charge, are used to define the natural bonding orbitals. To complete the span of valence space, the bonding NBO (σ) and the antibonding NBO (σ^*) are defined as follows:

$$\sigma_{AB} = C_A h_A + C_B h_B, \tag{6}$$

$$\sigma^*_{AB} = C_A h_A - C_B h_B. \tag{7}$$

Here, h_A and h_B are natural hybrid valence orbitals, whereas C_A and C_B are the corresponding polarization coefficients.

Table 4. Values of the natural charges (in a.u.) and the natural electron configurations for the isolated HCFC-124 and in its complex forming geometry. All calculations have been obtained at the ωB97XD/6-311G(d) level of theory.

Systems	Atom	Natural charge	Natural electron configuration
C_2HClF_4	Cl	−0.027	[core]3*s*(1.86)3*p*(5.15)3*d*(0.01)4*p*(0.01)
	F1	−0.340	[core]2*s*(1.83)2*p*(5.51)
	F2	−0.347	[core]2*s*(1.84)2*p*(5.51)
	F3	−0.354	[core]2*s*(1.84)2*p*(5.51)
	F4	−0.353	[core]2*s*(1.84)2*p*(5.51)
	C1	1.083	[core]2*s*(0.80)2*p*(2.04)3*s*(0.01)3*p*(0.05)3*d*(0.02)
	C2	0.095	[core]2*s*(1.05)2*p*(2.82)3*p*(0.02)3*d*(0.01)
	H	0.243	1*s*(0.75)
C_2HClF_4/CNT	Cl	−0.020	[core]3*s*(1.86)3*p*(5.14)3*d*(0.01)4*p*(0.01)
	F1	−0.351	[core]2*s*(1.83)2*p*(5.49)
	F2	−0.345	[core]2*s*(1.84)2*p*(5.50)3*d*(0.01)
	F3	−0.346	[core]2*s*(1.84)2*p*(5.50)3*d*(0.01)
	F4	−0.342	[core]2*s*(1.84)2*p*(5.50)3*d*(0.01)
	C1	1.061	[core]2*s*(1.03)2*p*(2.76)3*s*(0.01)3*p*(0.02)3*d*(0.01)
	C2	0.167	[core]2*s*(0.76)2*p*(2.11)3*p*(0.04)3*d*(0.02)
	H	0.186	1*s*(0.81)
C_2HClF_4/SiCNT	Cl	−0.003	[core]3*s*(1.86)3*p*(5.13)3*d*(0.01)4*p*(0.01)
	F1	−0.332	[core]2*s*(1.83)2*p*(5.49)
	F2	−0.345	[core]2*s*(1.84)2*p*(5.50)3*d*(0.01)
	F3	−0.342	[core]2*s*(1.84)2*p*(5.50)3*d*(0.01)
	F4	−0.351	[core]2*s*(1.84)2*p*(5.50)3*d*(0.01)
	C1	1.089	[core]2*s*(0.80)2*p*(2.04)3*s*(0.01)3*p*(0.05)3*d*(0.02)
	C2	0.090	[core]2*s*(1.06)2*p*(2.82)3*p*(0.02)3*d*(0.01)
	H	−0.181	1*s*(0.75)
C_2HClF_4/SiCGeNT	Cl	−0.003	[core]3*s*(1.86)3*p*(5.12)3*d*(0.01)4*p*(0.01)
	F1	−0.345	[core]2*s*(1.84)2*p*(5.50)
	F2	−0.338	[core]2*s*(1.84)2*p*(5.50)3*d*(0.01)
	F3	−0.346	[core]2*s*(1.84)2*p*(5.50)3*d*(0.01)
	F4	−0.342	[core]2*s*(1.84)2*p*(5.50)3*d*(0.01)
	C1	1.086	[core]2*s*(0.80)2*p*(2.04)3*s*(0.01)3*p*(0.05)3*d*(0.02)
	C2	0.095	[core]2*s*(1.05)2*p*(2.82)3*p*(0.02)3*d*(0.01)
	H	0.246	1*s*(0.75)

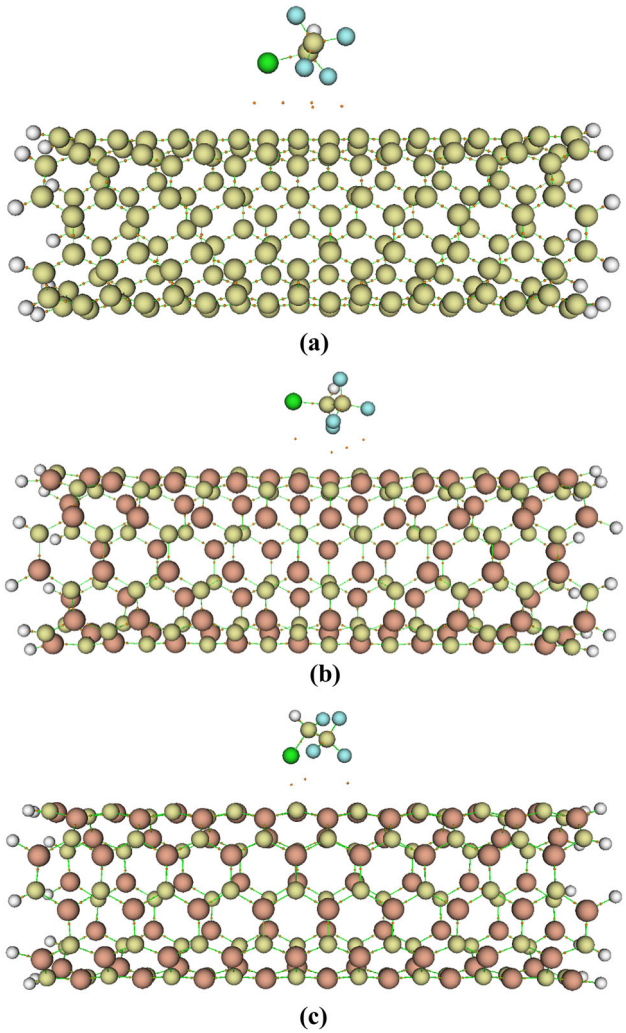

Figure 6. Bond critical point (BCP) diagrams for (**a**) HCFC-124/CNT, (**b**) HCFC-124/SiCNT and (**c**) HCFC-124/SiCGeNT systems. The orange dots denote the BCPs.

In the present study, NBO calculations were carried out to determine various types of bond orders as follows:

$$I_{\mathrm{AB}} = \sum_{i} \eta_i \sum_{a\in \mathrm{A}} \sum_{b\in \mathrm{B}} 2C_{a,i}C_{b,i}S_{a,b} = 2\sum_{a\in \mathrm{A}} \sum_{b\in \mathrm{B}} P_{a,b}S_{a,b}, \tag{8}$$

$$\begin{aligned} I_{\mathrm{AB}} &= I^{\alpha}_{\mathrm{AB}} + I^{\beta}_{\mathrm{AB}} \\ &= 2\sum_{a\in \mathrm{A}} \sum_{b\in \mathrm{B}} \left[(P^{\alpha}S)_{ba}(P^{\alpha}S)_{ab} + \left(P^{\beta}S\right)_{ba}\left(P^{\beta}S\right)_{ab} \right], \end{aligned} \tag{9}$$

$$I_{\mathrm{AB}} = \sum_{a\in \mathrm{A}} \sum_{b\in \mathrm{B}} P^2_{ab}. \tag{10}$$

These calculations include the Mulliken bond order [56] (equation 8), the Mayer bond order [57–59] (equation 9) and the Wiberg bond index (WBI) in the Löwdin orthogonalized basis [60,61] (equation 10). In these equations, P and S are density and overlap matrices, respectively. Mulliken and Mayer's bond orders are sensitive to the basis set, especially for the basis sets that include the diffuse functions. On the other hand, the Wiberg bond order is less susceptible to changes in the basis set. Table 3 reports the bond order values obtained from these three different approaches. Since WBI bond orders are presumed to be more accurate, we discuss the bond orders that are obtained through Wiberg's analysis. We can see that the Cl–C (or Cl–Ge) bond order of HCFC-124/SiCNT and HCFC-124/SiCGeNT are more than two times, greater than those obtained for the HCFC-124/CNT complex, indicating that the interaction between the HCFC-124 and SiCNT or SiCGeNT is much stronger than CNT. Furthermore, the bond order values also indicate that the interaction of the gas molecule with the CNT nanotube can be classified as physisorption. Therefore, these results may also be served to understand the adsorption on CNT (cf. table 1).

Table 5. QTAIM topological parameters for electron density $\rho(\mathbf{r})$, Laplacian of electron density $\nabla^2\rho(\mathbf{r})$, kinetic electron density $G(\mathbf{r})$, potential electron density $V(\mathbf{r})$, eigen values of Hessian matrix (λ) and bond ellipticity index (ε) at the BCPs of the HCFC-124 and CNT, SiCNT and SiCGeNT complexes. All values have been obtained at the ωB97XD/6-311G(d) level of theory and NBO analysis.

Systems	Bond	ρ	$\nabla^2\mathbf{r}$	$G(\mathbf{r})$	$V(\mathbf{r})$	$G(\mathbf{r})/V(\mathbf{r})$	λ_1	λ_2	λ_3	ε
C_2HClF_4/CNT	Cl....C	0.0051	0.0159	0.0031	−0.0023	1.3727	−0.0012	−0.0027	0.0198	1.2687
	F1....C	0.0049	0.0152	0.0030	−0.0022	1.3510	−0.0009	−0.0023	0.0185	1.4562
	C1....C	0.0063	0.0247	0.0051	−0.0041	1.2587	−0.0017	−0.0042	0.0306	1.4580
	C2....C	0.0063	0.0249	0.0051	−0.0040	1.2791	−0.0011	−0.0048	0.0308	3.2117
	F2....C	0.0060	0.0245	0.0051	−0.0040	1.2691	−0.0017	−0.0039	0.0302	1.2874
C_2HClF_4/SiCNT	Cl....C	0.0038	0.0103	0.0021	−0.0015	1.3329	−0.0015	−0.0019	0.0137	0.2762
	F1....C	0.0122	0.0325	0.0084	−0.0086	0.9732	−0.0058	−0.0074	0.0458	0.2580
	F2....C	0.0040	0.0159	0.0031	−0.0023	1.3583	−0.0020	−0.0026	0.0204	0.3100
	C1....C	0.0056	0.0218	0.0044	−0.0033	1.3227	−0.0014	−0.0037	0.0269	1.6038
C_2HClF_4/SiCGeNT	Cl....C	0.0082	0.0236	0.0049	−0.0039	1.2628	−0.0019	−0.0047	0.0303	1.4287
	F1....C	0.0080	0.0262	0.0059	−0.0053	1.1146	−0.0030	−0.0055	0.0347	0.8048
	F2....C	0.0067	0.0241	0.0050	−0.0040	1.2502	−0.0021	−0.0050	0.0312	1.4261

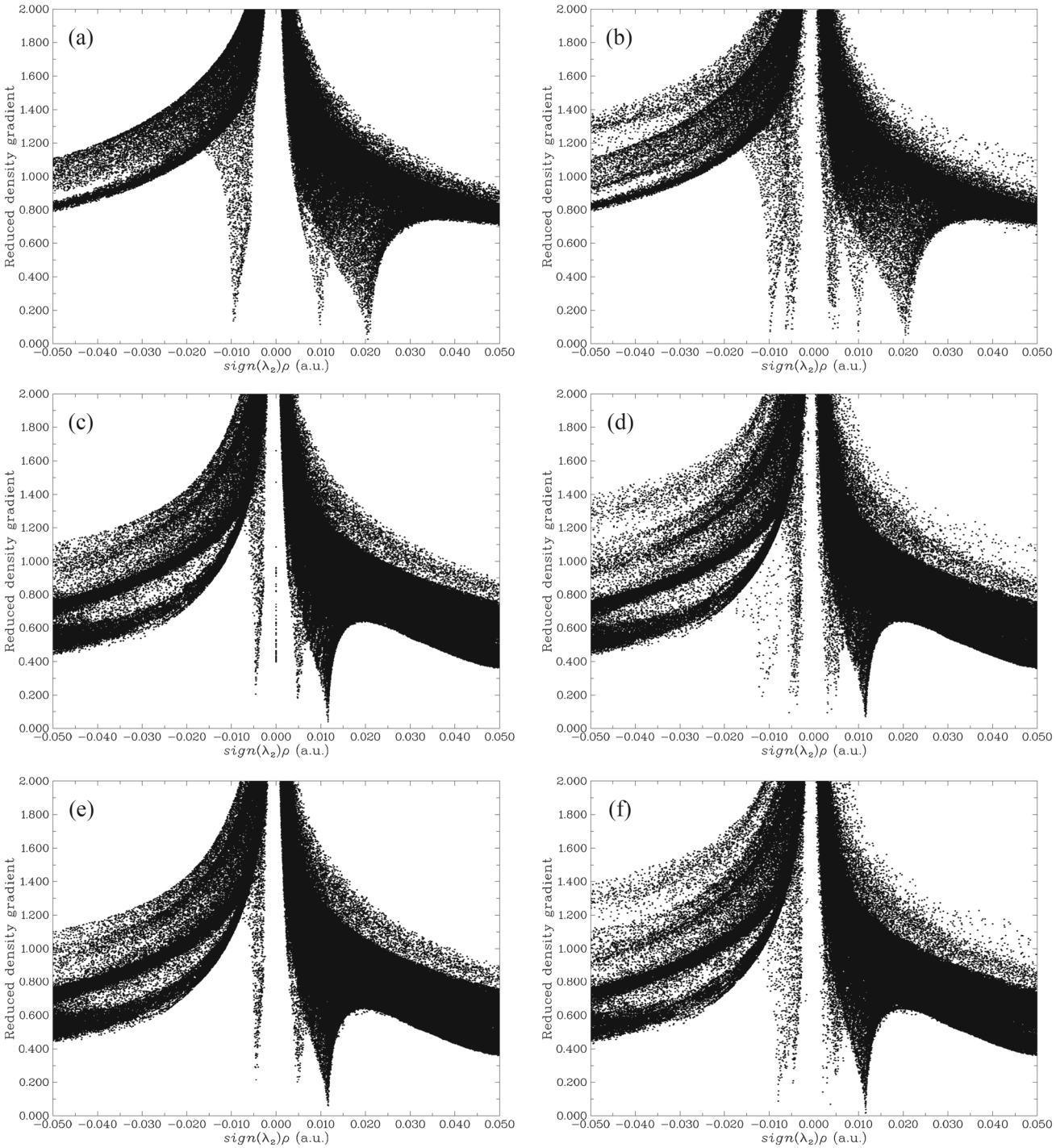

Figure 7. RDG (Y-axis) *vs.* sign(λ_2)ρ(**r**) (X-axis) plots for (**a**) CNT, (**b**) HCFC-124/CNT complex, (**c**) SiCNT, (**d**) HCFC-124/SiCNT complex, (**e**) SiCGeNT and (**f**) HCFC-124/SiCGeNT. The results are obtained at the ωB97XD/6-311G(d) level of theory.

Calculated natural charges and natural electron configuration are reported in table 4. Within the NBO consideration, the nature of the intermolecular interaction between the HCFC-124 molecule and the nanotubes are more intelligible. There is little or no changes in the electronic configuration of the valence shells for the atoms constituting the HCFC-124 molecule during adsorption, suggesting that the adsorption will be accomplished through van der Waals interactions.

3.4 *QTAIM analysis*

QTAIM analysis can be utilized to study the bond types and intermolecular interactions. A critical point of the electron density, including minimum, maximum, or saddle points, can belong to: (1) atomic critical point (ACP); (2) bond critical point (BCP); (3) ring critical point (RCP); and (4) cage critical point (CCP). The BCP's of the HCFC-124/CNT, HCFC-124/SiCNT and HCFC-124/SiCGeNT complexes at their optimized geometries are illustrated in figure 6. The electron density $\rho(\mathbf{r})$ and the Laplacian electron density $\nabla^2\rho(\mathbf{r})$ play a pivotal role in the QTAIM analysis since they can determine the segmentation and identify different types of chemical interactions. A BCP with negative values of Laplacian electron density and large values of electron density ($\rho(\mathbf{r}) > 10^{-1}$ a.u.) may be defined as a covalent bond. On the other hand, a positive value of $\nabla^2\rho(\mathbf{r})$ designates that the intermolecular interactions can be classified as closed-shell (either van der Waals or ionic) [62]. Since, the Laplacian electron density is always positive and $\rho(\mathbf{r})$ are $<10^{-1}$ a.u. for the HCFC-124/nanotube complexes, we may classify the interaction as closed-shell (table 5).

The values of Lagrangian kinetic energy $G(\mathbf{r})$ and potential energy density $V(\mathbf{r})$ can also be utilized to obtain insight into the nature of the intermolecular interaction. The ratio $G(\mathbf{r})/|V|(\mathbf{r})$ can act as a classifier of intermolecular interaction. If $G(\mathbf{r})/|V|(\mathbf{r}) < 0.5$, the nature of the interaction is covalent, and if $G(\mathbf{r})/|V|(\mathbf{r}) > 1$, the interaction can be classed as non-covalent. With the exception of the F1....C interaction in C_2HClF_4/SiCNT, all $G(\mathbf{r})/|V|(\mathbf{r})$ ratios are >1 as shown in table 5. These results indicate that there is a predominant non-covalent interaction between the HCFC-124 molecule and the nanotubes. In the case of SiCNT, much stronger non-covalent interactions can be identified.

Finally, the elliptical bond (ε), defined as $\varepsilon = \frac{\lambda_1}{\lambda_2} - 1, |\lambda_1| > |\lambda_2|$ is also a good indicator of bond strength [63]. A significant value of ε would indicate an unstable bond. Table 5 reports ε values for various bonds between HCFC-124 and the different nanotubes. Relatively small values of the elliptical bond signify the formation of stable bonds between the two fragments. It is interesting to note that the ε values are smaller in C_2HClF_4/SiCNT and C_2HClF_4/SiCGeNT complexes, in comparison to C_2HClF_4/CNT, which is in agreement with the NBO analysis.

As we have seen previously in this subsection that the interaction between the HCFC-124 molecule and the nanotubes may be non-covalent. Therefore, we further evaluated the interactions through a specific non-covalent analysis through reduced density gradient (RDG) and $\text{sign}\lambda_2(\mathbf{r})\rho(\mathbf{r})$ plots [64]. The NCI analysis can be performed by visualizing the different regions of the plot that signify different electrostatic interactions. RDG is defined as [64,65]:

$$\text{RDG} = \frac{1}{2(3\pi^2)^{1/3}} \frac{|\overline{\Delta\rho}(\mathbf{r})|}{\overline{\rho(\mathbf{r})}^{4/3}}. \tag{11}$$

The points in the RDG *vs.* $\text{sign}\lambda_2(\mathbf{r})\rho(\mathbf{r})$ plots that indicate strong interactions are located in the $\text{sign}\lambda_2(\mathbf{r})\rho(\mathbf{r}) < 0$ regions. The weaker van der Waals interactions are within the $\text{sign}\lambda_2(\mathbf{r})\rho(\mathbf{r}) \approx 0$ region. Finally, if many points are accumulated in the $\text{sign}\lambda_2(\mathbf{r})\rho(\mathbf{r}) > 0$ regions, then the interactions are of repulsive nature [64,65]. It should be noted that the bond strength is closely related to the density matrix $\rho(\mathbf{r})$ and $\text{sign}\lambda_2$. Low RDG and low electron density regions may correspond to the existence of non-covalent interactions between the components that are involved in the adsorption process.

The RDG and $\text{sign}\lambda_2(\mathbf{r})\rho(\mathbf{r})$ plots for the pristine nanocages and the optimized HCFC-124/nanocage complex are depicted in figure 7. Considering an isosurface as a reference (e.g., RDG = 0.5), numerous points are accumulated in the $\text{sign}\lambda_2(\mathbf{r})\rho(\mathbf{r}) \approx 0$ zone, after the adsorption of HCFC-124 molecule on a SiCNT and SiCGeNT. Therefore, the interactions can be classified as van der Waals. However, the interactions of HCFC-124 with SiCGeNT are stronger than those with either CNT or SiCNT. NCI analysis, in accordance with previous adsorption energy calculations, NBO and QTAIM analyses, indicate that the interaction between HCFC-124 and the Ge-doped nanotube is strong.

4. Conclusion

We have studied the intermolecular interactions between the HCFC-124 gas molecule, and CNT, SiCNT and SiCGeNT within the DFT framework. The molecular geometries have been optimized with the ωB97XD, M06-2X, CAM-B3LYP and B3LYP-D3 functionals in combination with a 6-311G(d) basis set. We find that the adsorption on Ge-doped nanotubes is highly favoured. In contrast, the undoped CNT shows the least affinity towards adsorption. To understand the nature of the intermolecular interactions between the adsorbate and the nanotube, we have carried out NBO, QTAIM and NCI analyses. The conclusions drawn from these approaches appear to be in good agreement. From the NBO analysis, we can deduce that the charge transfer between the two fragments does not play any significant role in the adsorption process. Instead, the QTAIM and NCI analyses show, van der Waals forces comprise the predominant intermolecular interactions for adsorption, especially on SiCGeNT. In fact, injecting a Ge atom in the SiCNT can be seen as a means for activating the surface of the nanotube for the adsorption of the HCFC-124. Consequently, SiCGeNT provide an excellent choice for building HCFC-124 nanosensors.

Acknowledgements

HYA thanks the Solid-State Theory Group, Physics Department, Università degli Studi di Milano, Milan, Italy, for providing computational facilities. SB and GB acknowledge the support of the European Regional Development Fund and the Republic of Cyprus through the Research Innovation Foundation (Cy-Tera project under the grant NEA YPODOMH/STPATH/0308/31, and NANO^{2}LAB project under the grant INFRASTRUCTURES/1216/0070).

References

[1] Fang X, Yao B, Vollmer M, Reimann S, Liu L, Chen L *et al* 2019 *Geophys. Res. Lett.* **46** 10034
[2] Secretariat UNEPO 2006 *Handbook for the Montreal protocol on substances that deplete the ozone layer: UNEP/Earthprint*
[3] Fahey D, Newman P A, Pyle J A, Safari B, Chipperfield M P, Karoly D *et al* 2018 *Scientific assessment of ozone depletion: 2018, global ozone research and monitoring project—Report no. 58* (Geneva, Switzerland: World Meteorological Organization)
[4] Solomon S, Manning M, Marquis M and Qin D 2007 *Climate change 2007: the physical science basis: working group I contribution to the fourth assessment report of the IPCC* (New York, USA: Cambridge University Press)
[5] Fahey D W and Hegglin M I 2011 *Scientific assessment of ozone depletion*: *2010, global ozone research and monitoring project—Report no. 52* (Geneva, Switzerland: World Meteorological Organization)
[6] Stocker T F, Qin D, Plattner G-K, Tignor M, Allen S K, Boschung J *et al* 2013 *Climate change 2013: the physical science basis. Contribution of working group I to the fifth assessment report of the Intergovernmental Panel on Climate Change* (United Kingdom and New York, USA: Cambridge University Press)
[7] Mohammadi M D and Hamzehloo M 2018 *Comput. Theor. Chem.* **1144** 26
[8] Nemati-Kande E, Abbasi M and Mohammadi M D 2019 *ChemistrySelect* **4** 2453
[9] Doust Mohammadi M and Abdullah H Y 2020 *ChemistrySelect* **5** 12115
[10] Mohammadi M D and Abdullah H Y 2020 *J. Mol. Model.* **26** 1
[11] Mohammadi M D and Abdullah H Y 2020 *Theor. Chem. Acc.* **139** 1
[12] Mohammadi M D and Abdullah H Y 2020 *Struct. Chem.* **32** 481
[13] Mohammadi M D, Salih I H and Abdullah H Y 2020 *Mol. Simul.* **46** 1405
[14] Mohammadi M D, Salih I H and Abdullah H Y 2020 *J. Comput. Biophys. Chem.* **20** 23
[15] Nemati-Kande E, Abbasi M and Mohammadi M D 2020 *J. Mol. Struct.* **1199** 126962
[16] Mohammadi M D and Abdullah H Y 2021 *Comput. Theor. Chem.* **1193** 113047
[17] Mohammadi M D, Abdullah H Y, Bhowmick S and Biskos G 2021 *Comput. Theor. Chem.* **1198** 113168
[18] Wilke K and Breuer H 1999 *J. Photochem. Photobiol. A: Chem.* **121** 49
[19] Saha D and Deng S 2009 *Langmuir* **25** 12550
[20] Botas J A, Calleja G, Sánchez-Sánchez M and Orcajo M G 2010 *Langmuir* **26** 5300
[21] Wang L-Q, Baer D R, Engelhard M H and Shultz A N 1995 *Surf. Sci.* **344** 237
[22] Bolton K 2003 *J. Mol. Struct.: Theochem.* **632** 145
[23] Wu Z, Li M, Howe J, Meyer III H M and Overbury S H 2010 *Langmuir* **26** 16595
[24] Yildirim T, Íñiguez J and Ciraci S 2005 *Phy.s Rev. B* **72** 153403
[25] Srinivasu K and Ghosh S K 2012 *J. Phys. Chem. C* **116** 25184
[26] Lin S, Ye X, Johnson R S and Guo H 2013 *J. Phys. Chem. C* **117** 17319
[27] Darwish A A, Fadlallah M M, Badawi A and Maarouf A A 2016 *Appl. Surf. Sci.* **377** 9
[28] Seif A and Azizi K 2016 *RSC Adv.* **6** 5079
[29] Seif A and Azizi K 2016 *RSC Adv.* **6** 58458
[30] Esrafili M D and Asadollahi S 2018 *J. Mol. Graph. Model.* **85** 323
[31] Lei W, Zhang H, Wu Y, Zhang B, Liu D, Qin S *et al* 2014 *Nano Energy* **6** 219
[32] Hjiri M, El Mir L, Leonardi S, Pistone A, Mavilia L and Neri G 2014 *Sens. Actuators B: Chem.* **196** 413
[33] Hohenberg P and Kohn W 1964 *Phys. Rev.* **136** B864
[34] Kohn W and Sham L J 1965 *Phys. Rev.* **140** A1133
[35] Pople J A, Gill P M and Johnson B G 1992 *Chem. Phys. Lett.* **199** 557
[36] Bickelhaupt F M and Baerends E J 2000 *Rev. Comput. Chem.* **15** 1
[37] Zhao Y and Truhlar D G 2008 *Theor. Chem. Acc.* **120** 215
[38] Chai J-D and Head-Gordon M 2008 *Phys. Chem. Chem. Phys.* **10** 6615
[39] Grimme S 2006 *J. Comput. Chem.* **27** 1787
[40] Grimme S, Antony J, Ehrlich S and Krieg H 2010 *J. Chem. Phys.* **132** 154104
[41] Grimme S, Ehrlich S and Goerigk L 2011 *J. Comput. Chem.* **32** 1456
[42] Yanai T, Tew D P and Handy N C 2004 *Chem. Phys. Lett.* **393** 51
[43] Kobayashi R and Amos R D 2006 *Chem. Phys. Lett.* **420** 106
[44] Goerigk L and Grimme S 2011 *Phys. Chem. Chem. Phys.* **13** 6670
[45] Ibach H and Lüth H 1995 *Solid state and physics* (Berlin: Springer) p 244
[46] Baker J 1987 *J. Comput. Chem.* **8** 563
[47] Frisch M, Trucks G, Schlegel H, Scuseria G, Robb M, Cheeseman J *et al* 2016 *Gaussian 16* (Wallingford, CT: Gaussian, Inc.)
[48] Lu T and Chen F 2012 *J. Comput. Chem.* **33** 580
[49] O'Boyle N M, Tenderholt A L and Langner K M 2008 *J. Comput. Chem.* **29** 839
[50] Boys S F and Bernardi F 1970 *Mol. Phys.* **19** 553
[51] Alkorta I, Trujillo C, Elguero J and Solimannejad M 2011 *Comput. Theor. Chem.* **967** 147
[52] Bredas J-L 2014 *Mater. Horiz.* **1** 17
[53] Foster A J and Weinhold F 1980 *J. Am. Chem. Soc.* **102** 7211
[54] Weinhold F and Landis C R 2001 *Chem. Educ. Res. Pract.* **2** 91

[55] Weinhold F and Landis C R 2012 *Discovering chemistry with natural bond orbitals* (New Jersey, USA: John Wiley & Sons Inc.)
[56] Mulliken R S 1955 *J. Chem. Phys.* **23** 1833
[57] Mayer I 1983 *Chem. Phys. Lett.* **97** 270
[58] Bridgeman A J, Cavigliasso G, Ireland L R and Rothery J 2001 *J. Chem. Soc. Dalton Trans.* **14** 2095
[59] Mayer I 2012 *Chem. Phys. Lett.* **544** 83
[60] Wiberg K B 1968 *Tetrahedron* **24** 1083
[61] Sizova O V, Skripnikov L V and Sokolov A Y 2008 *J. Mol. Struct.: Theochem.* **870** 1
[62] Matta C F 2006 *Hydrogen–hydrogen bonding: the non-electrostatic limit of closed-shell interaction between two hydro. Hydrogen bonding—new insights* (AA Dordrecht, The Netherlands: Springer) p 337
[63] Bohórquez H J, Boyd R J and Matta C F 2011 *J. Phys. Chem. A* **115** 12991
[64] Johnson E R, Keinan S, Mori-Sánchez P, Contreras-García J, Cohen A J and Yang W 2010 *J. Am. Chem. Soc.* **132** 6498
[65] Contreras-García J, Johnson E R, Keinan S, Chaudret R, Piquemal J-P, Beratan D N *et al* 2011 *J. Chem. Theory Comput.* **7** 625